Bucky-diamond versus onion-like carbon: End of graphitization

Qian Xu and Xiang Zhao*

Institute for Chemical Physics and Department of Chemistry, State Key Laboratory of Electrical Insulation and Power Equipment, Xi'an Jiaotong University, Xi'an 710049, China

(Received 28 May 2012; published 11 October 2012)

The graphitizing extent of nanodiamond has been studied by examining stabilities of all intermediate structures encountered in the graphitization process including bucky-diamond and onion-like carbon. The curves of enthalpy of formation imply that for nanodiamonds with various size and morphology, there are at least one or more peaks and valleys corresponding to the thermodynamically disfavored and favored structures, respectively. The unstable structures located at the peaks are indicated to be bucky-diamond and onion-like carbon. In contrast, the stable structures positioned along the valleys are variants of bucky-diamond. Furthermore, the difference in these structural stabilities is largely attributed to the relative contributions from both dangling bond energy and strain energy. The variants of bucky-diamond create a balance in those two aspects, and therefore become the thermodynamically favored structures and indicate the end of graphitization.

DOI: 10.1103/PhysRevB.86.155417 PACS number(s): 64.70.Nd, 68.35.bt, 61.46.Df

I. INTRODUCTION

Owing to the recent commercial availability of 5-nm nanodiamonds, nanoscale diamond particles have attracted enormous attention and exhibit promising perspectives in chemical and biomedical fields such as chemical catalysts,[1,2] drug delivery,[3] and biomedical markers.[4–7] These applications are largely attributed to the diverse properties of various phases including nanodiamond, bucky-diamond, and onion-like carbon (OLC).[7–9] Nevertheless, these various phases transform to each other under certain conditions, which will alter their surface morphologies and electronic structures, and may even change their assembly properties.[10] For example, graphitization causes phase transitions from nanodiamond to bucky-diamond to OLC, demonstrated in both aspects of experimental observation[11–16] and theoretical modeling.[16–20] At the same time, the reverse transformation from OLC to nanodiamond has also been observed experimentally[21–26] as well as modeled by molecular simulations.[27] Interestingly, in most cases of these two kinds of transformation, the final product is not the nanodiamond or OLC but the bucky-diamond, which is a carbon structure formed by a diamondlike core and single or multiple cagelike shells.[28,29]

In addition to experimental approaches, this phenomenon has also been studied by a number of thermodynamics models and molecular simulations in recent decades.[9,17,29–34] As early as 1990, Badziag *et al*. showed that in nanoscale, diamond may be more stable than graphite with a particle size of up to 5 nm based on a model of enthalpy of formation.[30] Later, Barnard *et al*. explicitly extended this familiar thermodynamic model to carbon nanoparticles including nanodiamond, bucky- diamond, carbon onion, and fullerene with respect to contributions not only from cohesive energy but also from strain energy and dangling bonds energy, leading to a relaxed nanodiamond occupying the stability "window" between ∼1.9 and ∼5.2 nm, as well as bucky-diamond coexisting with carbon onions in ∼1.7–2.0 nm and with nanodiamond in ∼2.0–2.2 nm.[9,31,32] Meanwhile, Raty and Galli examined the stability of nanodiamond as a function of surface hydrogen coverage and of size by *ab initio* calculations and found that bucky-diamond was thermodynamically more stable than those with hydrogenated nanodiamond at ∼3 nm.[35] All these results indicate that bucky-diamond is the thermodynamically preferred carbon nanostructure in a certain range of size. Additionally, the graphitization process on the (111) surface was recently revealed to be induced by the dangling bonds based on density functional theory computations, and meanwhile a criterion for the bond rupture process was also proposed.[36] Later, this proposed mechanism was supported by the studies of Petit *et al*. on the early stages of surface graphitization using x-ray photoelectron spectroscopy.[29] Such a bond rupture criterion greatly facilitates further theoretical explorations on graphitization.

However, one fundamental question, which has not yet been fully answered, is why in most cases the final product of structural transformations among nanodiamonds, bucky-diamond, and OLC is not the original nanodiamond or thoroughly graphitized product of OLC but the partial graphitized product of bucky-diamond with one or more shells. In other words, when does graphitization end?

In this paper, thermodynamics stability of intermediate carbon particles appearing during the graphitization process from clean nanodiamond to bucky-diamond to OLC was investigated by modifying the familiar thermodynamics model to a universal form. As surface hydrogenation may prevent the graphitization of nanodiamond,[36–38] only the clean carbon nanoparticles have been considered here.

II. METHODS

A. Enthalpy of formation computations

Phase stability of a carbon nanoparticle is estimated based on the enthalpy of formation on the basis of earlier works by Barnard *et al*.[9,31,32] The enthalpy of formation of fullerenes and carbon onions $[\Delta H_f^0(F)]$ as well as clean nanodiamond $[\Delta H_f^0(D)]$ was previously expressed in terms of the C-C bond energy E_{CC} and dangling bond energy E_{DB}, such

that

$$\frac{\Delta H_f^0(D)}{N_{\rm C}} = 2E_{\rm CC}^D + \frac{N_{\rm DB}}{N_{\rm C}}\left(E_{\rm DB}^D - \frac{1}{2}E_{\rm CC}^D + \Delta H_f^0({\rm DB})\right) + \Delta H_f^0({\rm C}), \quad (1)$$

$$\frac{\Delta H_f^0(F)}{N_{\rm C}} = \frac{3}{2}E_{\rm CC}^F + \Delta H_f^0({\rm C}) + \frac{E_{\rm strain}^F}{R^2} + \frac{1}{2}E_{\rm CC}^{\rm vdW}, \quad (2)$$

where $N_{\rm C}$ is the number of carbon atoms, $N_{\rm DB}$ is the number of dangling bonds, $E_{\rm CC}^D$ is the C-C bond energy in nanodiamond, $E_{\rm CC}^F$ is the C-C bond energy in fullerene and carbon onions, $E_{\rm CC}^{\rm vdW}$ is the *van der Waals* attraction between graphite sheets, $E_{\rm strain}^F$ is the contributions from strain energy, and $\Delta H_f^0({\rm C})$ is the standard enthalpy of formation of carbon at 298.15 K.

In the present study, treatments of (1) and (2) are modified to a universal form to evaluate the enthalpy of formation of each associated carbon nanoparticle in the graphitization process including nanodiamond, bucky-diamond, OLC, and other intermediate structures. First, according to the coordinate number of carbon atoms, the term $E_{\rm CC}$ is divided into three terms: $E_{\rm CC}^{sp}$, $E_{\rm CC}^{sp^2}$, and $E_{\rm CC}^{sp^3}$, respectively corresponding to the twofold, threefold, and fourfold carbon atoms. In this transformation, $E_{\rm CC}^{sp^2}$ and $E_{\rm CC}^{sp^3}$ are in accord with the original terms of $E_{\rm CC}^F$ and $E_{\rm CC}^D$; N_{sp}, N_{sp^2}, and N_{sp^3} are the number of carbon atoms with twofold, threefold, and fourfold hybridization, respectively. In this way, carbon structures simultaneously including twofold, threefold, and fourfold carbon atoms can be handled. Secondly, as the strain energy term of $E_{\rm strain}^F$ was used to describe the strain energy of a single carbon cage according to the proposition of Barnard *et al.*,[32] for the case of OLC formed by fullerenes and of bucky-diamond surrounded by $N_{\rm shells}$ fullerenes, it is reasonable to roughly assume that its strain energy is equal to $N_{\rm shells}$ times of the strain energy of a single carbon cage. Thus, a coefficient of $N_{\rm shells}$ is introduced and (1) and (2) become

$$\frac{\Delta H_f^0(D)}{N_{\rm C}} = \frac{N_{sp}}{N_{\rm C}}E_{\rm CC}^{sp} + \frac{N_{sp^2}}{N_{\rm C}}E_{\rm CC}^{sp^2} + \frac{N_{sp^3}}{N_{\rm C}}E_{\rm CC}^{sp^3} + \Delta H_f^0({\rm C}) + \frac{N_{\rm DB}}{N_{\rm C}}\left[E_{\rm DB}^D + \Delta H_f^0({\rm DB})\right] + N_{\rm shells}\frac{E_{\rm strain}^F}{R^2} + \frac{1}{2}E_{\rm CC}^{\rm vdW}. \quad (3)$$

The parameters used in the present work are as follows: $E_{\rm CC}^{sp^2} = 5.207$ eV, $E_{\rm CC}^{sp^3} = 3.855$ eV, $\Delta H_f^0({\rm C}) = 7.432$ eV, $E_{\rm DB}^D = 1.619$ eV, $E_{\rm strain}^F = 5.19$ eV, and $E_{\rm CC}^{\rm vdW} = 0.056$ eV, which are previously calculated from the result of VASP calculations and employed by Barnard *et al.*;[31,32] $\Delta H_f^0({\rm DB}) = 3.855$ eV as $\Delta H_f^0({\rm DB})$ is equal to the dissociation energy of the C-C bond; N_{sp}, N_{sp^2}, N_{sp^3}, $N_{\rm DB}$, $N_{\rm C}$, and $N_{\rm shells}$ are determined in the individual calculations; $E_{\rm CC}^{sp} = E_{\rm CC}^{sp^3}$ in this work for the twofold carbon atoms which are located on the (100) surfaces possess two C-C single bonds and two dangling bonds, and the numerical value of dangling bond is equal to that of C-C single bond.

However, a novel carbon structure will be encountered in the graphitization process, which we named "variant-bucky-diamond" in this work. It is a variant of bucky-diamond, appearing in the structure transformation from nanodiamond to bucky-diamond and from bucky-diamond to OLC, where only part of the carbon bonds on the interface between the innermost cage and the diamondlike core exist, and the other parts of the carbon bonds are broken. In order to correctly estimate the enthalpy of formation of the variant-bucky-diamond, we further extend formula (3). First, the dangling bonds are determined by satisfying either one of the following two criteria: if one atom is threefold and all three bonded atoms are fourfold, then the atom is considered to possess one dangling bond; if one atom is twofold and the two bonded atoms are fourfold, then the atom is deemed to have two dangling bonds. The former criterion is proposed for discerning the dangling bonds on the (111) surfaces and subsurfaces and the latter one is for distinguishing the dangling bonds on the (100) surfaces and subsurfaces, where the subsurfaces are gradually exposed during the graphitization process. In this way, the parameter $N_{\rm DB}$ can therefore be quantitatively obtained. Secondly, for variant-bucky-diamond, the strain energy of carbon cages can be assumed to be an accumulation of the contributions of every graphited carbon atom and therefore its value can be evaluated by summing up these contributions all over the graphited atoms, where the graphited atoms are the threefold atoms connected by π-π bonds and no dangling bond. Then, (3) becomes

$$\frac{\Delta H_f^0(D)}{N_{\rm C}} = \frac{N_{sp}}{N_{\rm C}}E_{\rm CC}^{sp} + \frac{N_{sp^2}}{N_{\rm C}}E_{\rm CC}^{sp^2} + \frac{N_{sp^3}}{N_{\rm C}}E_{\rm CC}^{sp^3} + \Delta H_f^0({\rm C}) + \frac{N_{\rm DB}}{N_{\rm C}}\left[E_{\rm DB}^D + \Delta H_f^0({\rm DB})\right] + \frac{N_{\rm shells}}{N_{\rm C}}\sum_{\rm graphited\ atoms}\frac{E_{\rm strain}^F}{R^2} + \frac{1}{2}E_{\rm CC}^{\rm vdW}. \quad (4)$$

Similarly, van der Waals attraction between nearby shells is assumed to be the sum of contributions from the graphited atoms and therefore the term $E_{\rm CC}^{\rm vdW}$ is calculated only for the graphited atoms:

$$\frac{\Delta H_f^0(D)}{N_{\rm C}} = \frac{N_{sp}}{N_{\rm C}}E_{\rm CC}^{sp} + \frac{N_{sp^2}}{N_{\rm C}}E_{\rm CC}^{sp^2} + \frac{N_{sp^3}}{N_{\rm C}}E_{\rm CC}^{sp^3} + \Delta H_f^0({\rm C}) + \frac{N_{\rm DB}}{N_{\rm C}}\left[E_{\rm DB}^D + \Delta H_f^0({\rm DB})\right] + \frac{N_{\rm shells}}{N_{\rm C}}\sum_{\rm graphited\ atoms}\frac{E_{\rm strain}^F}{R^2} + \frac{1}{2}\frac{N_{\rm graphited\ atoms}}{N_{\rm C}}E_{\rm CC}^{\rm vdW}. \quad (5)$$

In the following study, formula (5) is employed to estimate the enthalpy of formation of carbon nanoparticles.

B. Molecular simulation details

In this work, nanodiamond particles are constructed by cutting from ideal diamond crystals, with two morphologies of octahedral and truncated octahedral. Then, the simulation of graphitization follows the criterion proposed in our previous study.[36] In short, if one atom (atom A) on the (111) surfaces is fourfold atom bonded with three threefold atoms on the same surface and one fourfold atom (atom B) on the inner shell,

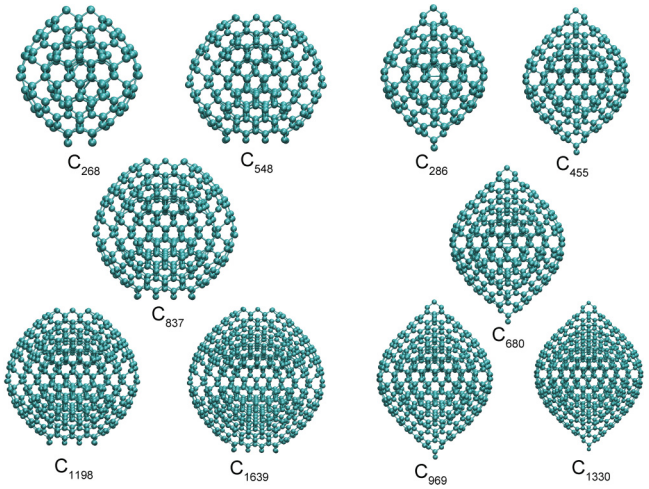

FIG. 1. (Color online) Examples of fully graphitized nanodiamonds with truncated octahedral shape (C_{268}, C_{548}, C_{837}, C_{1198}, and C_{1639}) and octahedral shape (C_{286}, C_{455}, C_{680}, C_{969}, and C_{1330}).

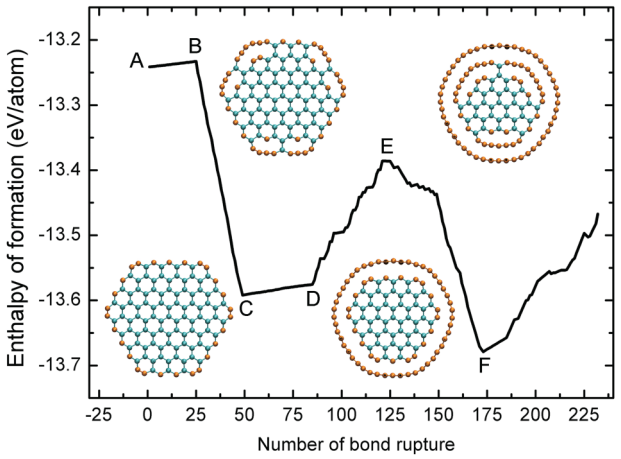

FIG. 2. (Color online) Enthalpy of formation of the intermediate carbon structures encountered in the graphitization process of nanodiamond C_{837} as well as four intermediaries in sectional view (orange for the threefold atoms and green for the fourfold atoms).

then the covalent bond connecting atom A and atom B will rupture. Furthermore, graphitization and exfoliation are most likely to take place preferentially in the area adjacent to the (111)/(111) edge. In addition, we assume the bonds rupture one after another, even for the equivalent bonds. Moreover, in order to evaluate the curvature of each graphited atom in the term $\sum_{\text{graphited atoms}} (E^F_{\text{strain}}/R^2)$, structural relaxation was carried out for each structure by a MM2 force field using the TINKER molecular modeling package.[39]

These criteria and computational methods have been verified in our previous study examining the graphitization process, which describes the bond rupture and obtains a result consistent with experimental observations and molecular simulations.[36] In particular, such criteria are concluded from the quantum-mechanical simulations and can correctly reflect the contribution of electrons and dangling bonds. Nevertheless, due to the restriction of computational capabilities, it has not been easy to deal with molecules with thousands of atoms by quantum-mechanical methods until now. Even so, such attempts of pure quantum simulations are being carried on and will be discussed in our future work. In the present work, we use formula (5) to give a preliminary estimation on the thermodynamic stability of the intermediate structures. Furthermore, in order to improve the accuracy of the estimated curvature of each graphited atom, which corresponds to the parameters of R in formula (5), a force field based method is performed. Finally, such a phenomenological model not only evidently indicates the end of graphitization, but also intuitively exhibits the influential factors related to the stability of those carbon nanostructures. Examples of the fully graphitized nanodiamonds are shown in Fig. 1.

III. RESULTS AND DISCUSSION

First, we focus on the intermediate carbon nanostructures appearing in the graphitization process of truncated octahedral nanodiamond C_{837} (2.2 nm). The atomic enthalpy of formation of these intermediaries is illustrated in Fig. 2, in a manner of curve which represents the relationship of the enthalpy of formation and the number of bond rupture. Notably, the curve is composed of several lines, where the same line indicates the broken of the equivalent bonds, one after another. Thus, due to the distinction of bond rupture in different lines, the curve goes upward in some stages and downward in other stages, leading to the formation of two valleys. The first valley is located at the number of bond rupture 50–80, while the second one is at 175. These two valleys suggest two thermodynamic stable morphologies in all intermediaries, which suffer different degrees of bond rupture and thus possess a distinct number of carbon cages. As presented in Fig. 2, the intermediate structures in the first valley are surrounded by one carbon cage, while the structures in the second valley are encircled by two cages. Furthermore, these two valleys are separated by a large energy barrier of ~0.2 eV/atom, suggesting that structural transition between these two morphologies requires high extra energy to overcome the energy barrier, and consequently, carbon nanostructures with one or more cages could coexist.[40] Meanwhile, the energy barrier suggests that the graphitization on the surface only requires a minor activated energy that can be achieved in a lower temperature, while the further graphitization on the inner diamond core needs a higher temperature, leading to the conclusion that the extent and dynamics of graphitization depend on the temperature, which is in agreement with recent experimental observations.[29]

Interestingly, bucky-diamonds and OLCs take up the peaks of the curve, indicating that they have a relatively low enthalpy of formation and no thermodynamics advantage in comparison to the phases in the valleys. In contrast, the energy favored structure in the valley is variant-bucky-diamond.

In order to determine the factors affecting the stability of carbon nanostructures in the graphitization process, the covalent bonds, dangling bonds, and the movement of relative energies are therefore carefully examined. As expected, the covalent bonds decrease linearly as the number of bond ruptures increases, as shown in Fig. 3(a). Furthermore, as presented in Fig. 3(b), the number of fourfold atoms decreases while the number of threefold atoms increases, in accordance with the features of graphitization that sp^3 carbon atoms

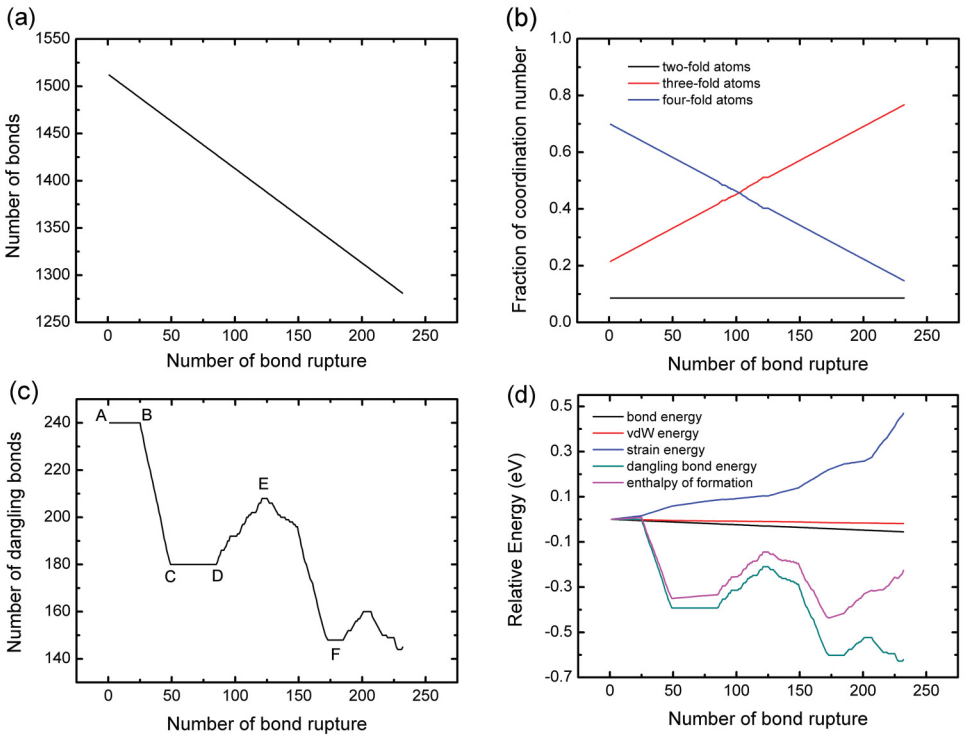

FIG. 3. (Color online) Graphitization process of nanodiamond C_{837}: (a) number of bonds, (b) fraction of coordination number, (c) number of dangling bonds, and (d) relative energy as number of bond rupture.

transform into sp^2 carbon atoms and with the experimental measured fractions on the early stages of graphitization.[29] In addition, the fraction of twofold atoms stays the same in the graphitization process, as the twofold atoms located on the (100) surface are unchanged. It should be noted that carbon atoms on the (100) surfaces will not participate in the graphitization process, and the twofold atoms on the (100) surfaces have a negligible impact on the relative value of enthalpy of formation.[36] Thus, the reconstruction process on the (100) surfaces is not considered and the outcomes of current studies will not be affected.

The movements of relative energies are illustrated in Fig. 3(d). It is clear that the enthalpy of formation is dominated by the two factors, dangling bond energy and strain energy, while contributions from bond energy and van der Waals are very small. Notably, dangling bond energy shares the same movement tendency with total energy in the entire graphitization process, suggesting that the dangling bond is the decisive factor to the enthalpy of formation. On the other hand, the impact of strain energy increases as the graphitization continues, since the effects of strain energy become more evident for the smaller carbon cages encountered at the later stages of the graphitization process.

However, the number of dangling bonds is not linear dependent on the number of bond ruptures. In turn, similar to the situation of enthalpy of formation, the number of dangling bonds has a distinct tendency in different stages of graphitization. For example, in line B-C in Fig. 3(c), the number of dangling bonds decreases while in line D-E, the number of dangling bonds increases. Therefore, the dangling bond energy shows valleys and peaks too, as illustrated in Fig. 3(d).

Furthermore, the relative number of dangling bonds is found to be associated with the specific bond rupture process. As addressed in Figs. 4(a)–4(c), bond *A*-*B* (colored red) breaks, leading to both atom *A* and atom *B* becoming threefold

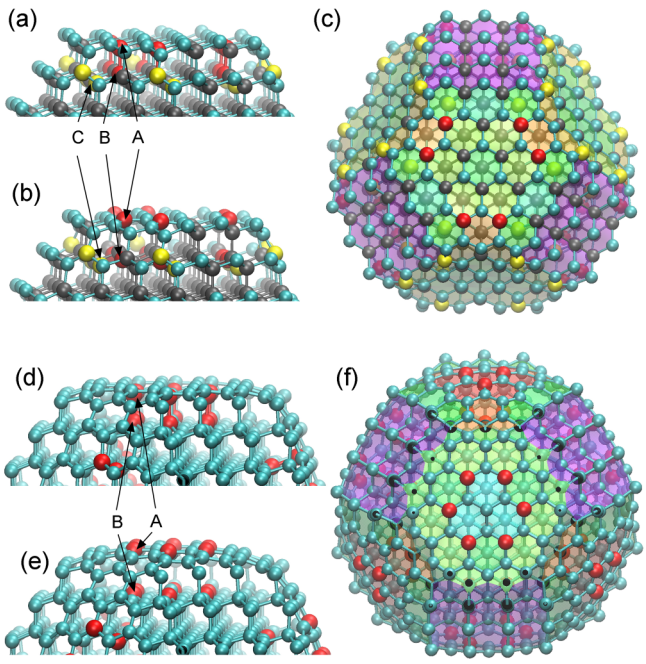

FIG. 4. (Color online) Examples of the dangling bonds before [(a), (d)] and after [(b), (c), (e), and (f)] the bond rupture process: (a), (b), (d), and (e) in side view; (c) and (f) in top view. (a)–(c) correspond to line B-C in Fig. 3(c)); (d)–(f) represent line D-E in Fig. 3(c).

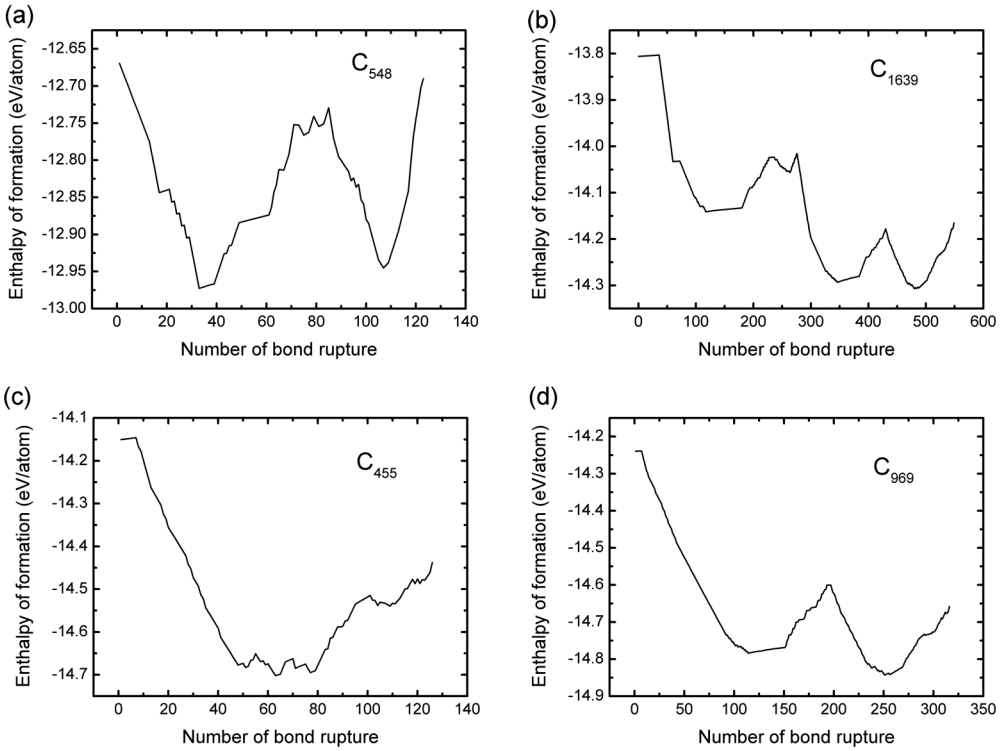

FIG. 5. Enthalpy of formation as number of bond rupture of truncated octahedral nanodiamonds (a) C_{548} and (b) C_{1639} as well as octahedral nanodiamonds (c) C_{455} and (d) C_{969}.

atoms and may combine nearby atoms on the same surface to form π bonds. In detail, on the one hand, each of the three atoms connected to atom A on the same surface possesses one dangling bond before rupture and will lose them after, causing a decrease of three dangling bonds in total. On the other hand, for the atoms in the inner cages such as atom B, its coordination number changes from four to three in the rupture process. But as shown in Fig. 4(c), since one of the atoms connected to B has already suffered bond rupture and possesses three connected atoms, which is atom C (colored yellow) in this case, atoms B and C will form a new π bond rather than form new dangling bonds. Therefore, as a total effect of these two aspects, the rupture of bond A-B gives rise to a reduction of three dangling bonds.

In another situation, the bond rupture process corresponding to line D-E in Fig. 3(c) causes the number of dangling bonds to increase. As illustrated in Figs. 4(d)–4(f), bond A-B breaks. Consequently, for atom A, since each of the atoms connected to atom A on the same surface has previously formed π bonds without any dangling bonds, the bond rupture has no effect on these atoms. And for atom B, every atom connected to atom B on the same surface is a fourfold atom before the rupture and after, leading to only one new dangling bond forming at the location of atom B. As a consequence, the rupture of bond A-B brings out one new dangling bond.

Since the number of dangling bonds is not monotonic, the valleys and peaks of the curve of enthalpy of formation therefore form. Further, because bucky-diamond and OLC have more dangling bonds than variant-bucky-diamond, the former two structures locate at the peaks of the curve and the latter structure takes up the valleys.

The influence of particle size on enthalpy of formation is also examined by investigating truncated octahedral nanodiamonds C_{548} (1.8 nm) and C_{1639} (2.8 nm) as well as octahedral nanodiamonds C_{455} (2.0 nm) and C_{969} (2.8 nm). As illustrated in Fig. 5, several features are evident. First, as the size increases, more valleys appear. In the case of truncated octahedral nanodiamonds from C_{548} to C_{1639}, the number of valleys grows from two to three. Likewise, for octahedral nanodiamonds from C_{455} to C_{969}, the number of valleys increases from one to two. Secondly, for the larger nanodiamonds such as C_{1639} and C_{969}, the first valley has no more of a thermodynamic advantage than the other valleys, resulting in the final product of the variant-bucky-diamond always possessing more than one carbon cage.

The curve of enthalpy of formation and the variant-bucky-diamond structures greatly facilitate the understanding of some experimental results. For instance, as the thermodynamics-favored structure is variant-bucky-diamond rather than the nanodiamond and OLC, the transformations from either nanodiamond or OLC to variant-bucky-diamond are achievable. This is in agreement with the experimental observations that both the transformation from nanodiamonds to carbon onions and reverse transformation from carbon onions to nanodiamonds occur. Moreover, previous experiments revealed that the mechanism and extent of graphitization depend on temperature.[29,41] Nanodiamond transforms into bucky-diamond in a lower temperature. However, in a higher temperature, nanodiamond transforms into OLC. With the curve of enthalpy of formation, these phenomena can also be elucidated. The graphitization from nanodiamond to the first variant-bucky-diamond is likely to occur spontaneously, leading to a low initial temperature.

Nevertheless, the graphitization from the first valley to the next valleys requires remarkable active energy to overcome the energy barrier, thus a higher temperature is necessary. Furthermore, variant-bucky-diamond has an advantage over the enthalpy of formation and makes it the most probable experimental product. As illustrated in Figs. 4(b) and 4(d), the dangling bonds with unpaired electrons in the variant-bucky-diamond exist in the location of inner carbon shells, in agreement with the experimental measurement from NMR spectroscopy that nanodiamond has a core-shell structure within unpaired electrons probably in homogeneous distributions.[42–45] Meanwhile, in some experiments nanodiamond particles are reported to have a core-shell structure with an ordered diamond core covered by a disordered (amorphous) outer shell formed by the mixed sp^2/sp^3 carbon atoms.[46] Such a disordered outer shell is consistent with the structural features of variant-bucky-diamond, as illustrated in Figs. 4(b) and 4(d).

IV. CONCLUSION

In conclusion, thermodynamic stabilities of the intermediate carbon nanoparticles in the graphitization process of nanodiamonds are investigated. The curves of enthalpy of formation exhibit one or more valleys, indicating that the stable carbon nanoparticles possess one or more carbon cages, and graphitization will most probably end at the locations of valleys. The enthalpy of formation is determined by two factors: the dangling bond energy and strain energy. As the graphitization continues, the strain energy monotonically increases, while the number of dangling bonds and associated dangling bond energies increase in some bond rupture stages and decrease in other stages, which depends on the specific bond rupture process. Consequently, the valleys on the curve subsequently form and the carbon structures on the valleys are indicated to possess a variant-bucky-diamond structure.

ACKNOWLEDGMENTS

This work has been supported by National Natural Science Foundation of China (21171138), and partially by the National Key Basic Research Program of China (2012CB720904) and Key Project in the National Science and Technology Pillar Program of China (2010BAK67B12). The Program package TINKER is also acknowledged.

*xzhao@mail.xjtu.edu.cn

[1] J. Zhang, D. S. Su, R. Blume, R. Schlögl, R. Wang, X. Yang, and A. Gajović, Angew. Chem., Int. Ed. **49**, 8640 (2010).
[2] D. M. Jang, Y. Myung, H. S. Im, Y. S. Seo, Y. J. Cho, C. W. Lee, J. Park, A.-Y. Jee, and M. Lee, Chem. Commun. (Cambridge) **48**, 696 (2012).
[3] X. Q. Zhang, R. Lam, X. Xu, E. K. Chow, H.-J. Kim, and D. Ho, Adv. Mater. **23**, 4770 (2011).
[4] A. S. Barnard, Analyst **134**, 1751 (2009).
[5] Y. R. Chang, H. Y. Lee, K. Chen, C. C. Chang, D. S. Tsai, C. C. Fu, T. S. Lim, Y. K. Tzeng, C. Y. Fang, C. C. Han, H. C. Chang, and W. Fann, Nat. Nanotechnol. **3**, 284 (2008).
[6] K. B. Holt, Philos. Trans. R. Soc. London A **365**, 2845 (2007).
[7] V. N. Mochalin, O. Shenderova, D. Ho, and Y. Gogotsi, Nat. Nanotechnol. **7**, 11 (2012).
[8] A. S. Barnard, Diamond Relat. Mater. **15**, 285 (2006).
[9] A. S. Barnard, S. P. Russo, and I. K. Snook, J. Comput. Theor. Nanosci. **2**, 180 (2005).
[10] I. Kulakova, Phys. Solid State **46**, 636 (2004).
[11] V. L. Kuznetsov, A. L. Chuvilin, Y. V. Butenko, I. Y. Mal'kov, and V. M. Titov, Chem. Phys. Lett. **222**, 343 (1994).
[12] V. L. Kuznetsov, I. L. Zilberberg, Y. V. Butenko, A. L. Chuvilin, and B. Segall, J. Appl. Phys. **86**, 863 (1999).
[13] S. Tomita, T. Sakurai, H. Ohta, M. Fujii, and S. Hayashi, J. Chem. Phys. **114**, 7477 (2001).
[14] S. Tomita, A. Burian, J. C. Dore, D. LeBolloch, M. Fujii, and S. Hayashi, Carbon **40**, 1469 (2002).
[15] J. Qian, C. Pantea, J. Huang, T. W. Zerda, and Y. Zhao, Carbon **42**, 2691 (2004).
[16] L. Hawelek, A. Brodka, S. Tomita, J. C. Dore, V. Honkimaeki, and A. Burian, Diamond Relat. Mater. **20**, 1333 (2011).
[17] F. Fugaciu, H. Hermann, and G. Seifert, Phys. Rev. B **60**, 10711 (1999).
[18] J. H. Los, N. Pineau, G. Chevrot, G. Vignoles, and J.-M. Leyssale, Phys. Rev. B **80**, 155420 (2009).
[19] P. Ganesh, P. R. C. Kent, and V. Mochalin, J. Appl. Phys. **110**, 073506 (2011).
[20] S. P. Adiga, L. A. Curtiss, and D. M. Gruen, *Molecular Dynamics Simulations of Nanodiamond Graphitization* (Springer, New York, 2010).
[21] F. Banhart and P. M. Ajayan, Nature (London) **382**, 433 (1996).
[22] M. Zaiser, Y. Lyutovich, and F. Banhart, Phys. Rev. B **62**, 3058 (2000).
[23] F. Banhart, Rep. Prog. Phys. **62**, 1181 (1999).
[24] M. Zaiser and F. Banhart, Phys. Rev. Lett. **79**, 3680 (1997).
[25] S. Tomita, M. Fujii, S. Hayashi, and K. Yamamoto, Diamond Relat. Mater. **9**, 856 (2000).
[26] J. Y. Huang, Nano Lett. **7**, 2335 (2007).
[27] R. Astala, M. Kaukonen, R. M. Nieminen, G. Jungnickel, and T. Frauenheim, Phys. Rev. B **63**, 081402 (2001).
[28] J. Y. Raty, G. Galli, C. Bostedt, T. W. van Buuren, and L. J. Terminello, Phys. Rev. Lett. **90**, 037401 (2003).
[29] T. Petit, J.-C. Arnault, H. A. Girard, M. Sennour, and P. Bergonzo, Phys. Rev. B **84**, 233407 (2011).
[30] P. Badziag, W. S. Verwoerd, W. P. Ellis, and N. R. Greiner, Nature (London) **343**, 244 (1990).
[31] A. S. Barnard, S. P. Russo, and I. K. Snook, Phys. Rev. B **68**, 073406 (2003).
[32] A. S. Barnard, S. P. Russo, and I. K. Snook, J. Chem. Phys. **118**, 5094 (2003).
[33] N. Winter and F. Ree, J. Comput.-Aided Mol. Des. **5**, 279 (1998).
[34] M. Yu, I. Chaudhuri, C. Leahy, S. Y. Wu, and C. S. Jayanthi, J. Chem. Phys. **130**, 184708 (2009).
[35] J. Y. Raty and G. Galli, Nature Mater. **2**, 792 (2003).
[36] L. S. Li and X. Zhao, J. Chem. Phys. **134**, 044711 (2011).

[37] A. S. Barnard, S. P. Russo, and I. K. Snook, Int. J. Mod. Phys. B **17**, 3865 (2003).
[38] J. Y. Raty and G. Galli, J. Electroanal. Chem. **584**, 9 (2005).
[39] J. W. Ponder, TINKER—Software Tools for Molecular Design, V. 6.0.08, Saint Louis, 2011, http://dasher.wustl.edu/tinker/.
[40] V. L. Kuznetsov, A. L. Chuvilin, Y. V. Butenko, S. V. Stankus, R. A. Khairulin, and A. K. Gutakovskii, Chem. Phys. Lett. **289**, 353 (1998).
[41] Y. V. Butenko, V. L. Kuznetsov, A. L. Chuvilin, V. N. Kolomiichuk, S. V. Stankus, R. A. Khairulin, and B. Segall, J. Appl. Phys. **88**, 4380 (2000).
[42] X. Fang, J. Mao, E. M. Levin, and K. Schmidt-Rohr, J. Am. Chem. Soc. **131**, 1426 (2009).
[43] A. V. Fionov, A. Lund, W. M. Chen, N. N. Rozhkova, I. A. Buyanova, G. I. Emel'yanova, L. E. Gorlenko, E. V. Golubina, E. S. Lokteva, E. Osawa, and V. V. Lunin, Chem. Phys. Lett. **493**, 319 (2010).
[44] A. I. Shames, A. M. Panich, W. Kempinski, A. E. Alexenskii, M. V. Baidakova, A. T. Dideikin, V. Y. Osipov, V. I. Siklitski, E. Osawa, M. Ozawa, and A. Y. Vul, J. Phys. Chem. Solids **63**, 1993 (2002).
[45] M. Dubois, K. Guérin, E. Petit, N. Batisse, A. Hamwi, N. Komatsu, J. Giraudet, P. Pirotte, and F. Masin, J. Phys. Chem. C **113**, 10371 (2009).
[46] O. O. Mykhaylyk, Y. M. Solonin, D. N. Batchelder, and R. Brydson, J. Appl. Phys. **97**, 074302 (2005).